ELSEVIER

Neurobiology of Aging 22 (2001) 529–539

NEUROBIOLOGY OF AGING

www.elsevier.com/locate/neuaging

Hippocampal formation glucose metabolism and volume losses in MCI and AD

Susan De Santi[a,*], Mony J. de Leon[a,c], Henry Rusinek[b], Antonio Convit[a,c], Chaim Y. Tarshish[a], Alexandra Roche[a], Wai Hon Tsui[c], Emad Kandil[a], Madhu Boppana[a], Katherine Daisley[a], Gene Jack Wang[d], David Schlyer[e], Joanna Fowler[e]

[a]*Department of Psychiatry, New York University School of Medicine, New York, NY, USA*
[b]*Department of Radiology, New York University School of Medicine, New York, NY, USA*
[c]*The Nathan Kline Institute for Psychiatric Research, Orangeburg, NY, USA*
[d]*Department of Medicine, Brookhaven National Laboratory, Upton, NY, USA*
[e]*Department of Chemistry, Brookhaven National Laboratory, Upton, NY, USA*

Received 19 September 2000; received in revised form 19 February 2001; accepted 23 February 2001

Abstract

We used MRI volume sampling with coregistered and atrophy corrected FDG-PET scans to test three hypotheses: 1) hippocampal formation measures are superior to temporal neocortical measures in the discrimination of normal (NL) and mild cognitive impairment (MCI); 2) neocortical measures are most useful in the separation of Alzheimer disease (AD) from NL or MCI; 3) measures of PET glucose metabolism (MRglu) have greater diagnostic sensitivity than MRI volume. Three groups of age, education, and gender matched NL, MCI, and AD subjects were studied. The results supported the hypotheses: 1) entorhinal cortex MRglu and hippocampal volume were most accurate in classifying NL and MCI; 2) both imaging modalities identified the temporal neocortex as best separating MCI and AD, whereas widespread changes accurately classified NL and AD; 3) In most between group comparisons regional MRglu measures were diagnostically superior to volume measures. These cross-sectional data show that in MCI hippocampal formation changes exist without significant neocortical changes. Neocortical changes best characterize AD. In both MCI and AD, metabolism reductions exceed volume losses.

Keywords: PET; MRI; Mild cognitive impairment; Early diagnosis of Alzheimer's disease; Hippocampal formation

1. Introduction

The neuropathological changes of Alzheimer's disease (AD) (e.g. senile plaques, neurofibrillary tangles, and neuronal degeneration) have been identified in the brains of nondemented subjects who did not exhibit clinical evidence of AD during life [1–12]. In cognitively normal (NL) subjects [3,5,7–9,12] and in cases with mild cognitive impairment (MCI) [4,9,10,12–15] the entorhinal cortex and the hippocampus are the brain regions most consistently demonstrating AD lesions. Clinically diagnosed AD patients typically show additional pathology in neocortical areas [2,6,16–18]. These results suggest that AD pathology begins in the entorhinal cortex and hippocampus during a preclinical stage of the disease with the spread to neocortical sites that are associated with clinical detection [3,5,6].

Recent studies show MCI patients are at high risk for developing future AD (for review see [19–21]). Structural imaging studies consistently report atrophy of the hippocampus in MCI [22–25]. This atrophy is predictive of future AD [25–30] and appears to be focal [24]. Most recently, the volume of the entorhinal cortex has also been shown to predict AD among MCI subjects [31]. Among patients with clinically diagnosed AD, structural imaging studies show widespread changes; ventricular enlargement (see [32] for review) and cortical atrophy (see [33] for review) are well documented in this group. Recently, atrophy of the hippocampus [24,26,34–39] and entorhinal cortex [40–42] have also been reported.

AD has been extensively studied with FDG-PET and

* Corresponding author. Tel.: +1-212-263-5699; fax: +1-212-263-6991.

E-mail address: susan.desanti@med.nyu.edu (S. De Santi).

0197-4580/01/$ – see front matter
PII: S0197-4580(01)00230-5

neocortical regional glucose metabolism (MRglu) reductions are well documented [43–49]. However, sampling hippocampal MRglu in AD, typically conducted without MRI coregistration, has produced both positive [50–54], and negative [55–57] findings. Few PET studies of MCI exist and there is mixed evidence for temporal lobe MRglu reductions (medial, lateral, or both) [58–63]. Moreover, there are no reported comparisons between regional MRglu and MRI volume measures. Consequently, there are no cross-modality comparisons and it is unknown if MRglu alterations are independent of size change.

This paper uses coregistered FDG-PET and MRI scans to determine the atrophy corrected MRglu and volume of six temporal lobe subregions in groups of NL, MCI and AD patients. We demonstrate the diagnostic value of MRglu measures of the hippocampus and anterior parahippocampal gyrus (level of the entorhinal cortex) and hippocampal volume measurements in MCI; confirm the neocortical changes that characterize AD; and report on the generally superior diagnostic accuracy achieved with regional MRglu measures as compared with MRI volumes.

2. Subjects and methods

2.1. Subjects

Subjects were drawn from New York University (NYU) School of Medicine Alzheimer's Disease Core Center. Informed consent was obtained from all subjects (and when appropriate from the caregiver as well) at NYU and Brookhaven National Laboratories (BNL). Subjects received an extensive screening and diagnostic battery that included medical, neurologic, psychiatric, neuropsychological, and neuroradiological examinations. Subjects were excluded from this study if they had evidence of a significant neurological abnormality (e.g. stroke), psychiatric disorder (e.g. depression), significant medical conditions (e.g. uncontrolled hypertension or diabetes), or sensory impairment. Both the Global Deterioration Scale (GDS) [64], a seven-point rating scale assessing cognitive and functional capacity, and the Mini-Mental Status Examination (MMSE) [65] were administered to stage the study participants. Subjects were categorized as follows: NL subjects (GDS 1 and 2, n = 11), MCI (GDS 3, n = 15) and mild to moderately severe AD (GDS 4 and 5, n = 12). Further, MMSE scores < 24 excluded individuals from the NL and MCI categories. The diagnosis of AD was made according to the guidelines of the NINCDS-ADRDA criteria [66] and DSM IV [67]. The MCI diagnosis was based on the GDS and has been used in several prior studies predicting AD from MCI [20,26,68, 69]. (See Table 1 for demographic information). Four of the NL and 5 of the MCI patients were included in a previous MRI report [30].

Table 1
Demographic variables: mean (SD) and [range]

	NL $N = 11$	MCI $N = 15$	AD $N = 12$
% Females	42%	40%	50%
Age	76.5	74.6	76.1
	(5.4)	(6.7)	(7.0)
	[68–87]	[63–82]	[63–87]
Education	15.6	16.3	15.2
	(2.9)	(3.0)	(2.9)
	[12–18]	[8–18]	[12–18]
MMSE	29.1	28.5	20.3[a,b]
	(1.5)	(1.9)	(7.2)
	[25–30]	[24–30]	[5–30]

MMSE - Mini-Mental Status Examination.
[a] Significantly different from NL, $p < .001$.
[b] Significantly different from MCI, $p < .001$.

2.2. PET studies

Subjects received a PET scan at BNL using a Siemens CTI-931 scanner (Knoxville, TN) and 2-[^{18}F]fluoro-2-Deoxy-D-glucose (FDG) as the tracer. The scanner generated 15 axial tomographic slices covering 101 mm with an in-plane resolution of 6.2 mm full width at half maximum, and a cross slice resolution of 6.7 mm. The inter-slice distance was 6.75 mm. Images were reconstructed with the Hanning filter with a frequency cutoff of 0.5 cycles/pixel yielding 128×128 matrix with a pixel size of 1.56 mm. Each subject's head was positioned using two orthogonal laser beams and imaged with the scanner tilted 25° negative to the canthomeatal plane [22]. This plane runs approximately parallel to the long axis of the hippocampus. To reduce head movement during scanning, a molded plastic head holder was custom-made for each subject. Attenuation correction was obtained using transmission scans.

One hour prior to the FDG-PET scan, a radial artery catheter and contralateral antecubital venous lines were positioned. Subjects received 5–6 mCi of FDG intravenously. Arterial blood samples were obtained at standard intervals throughout the study to monitor glucose and ^{18}F levels in the blood. During the tracer uptake and scanning periods, the subjects lay supine in the machine with their eyes opened and ears unoccluded in a dimly lit room. Scanning commenced 35 minutes after isotope injection and lasted for 20 minutes. In order to improve the z-axis spatial resolution and isotope recovery we used two interleaved data acquisitions. After acquiring the first set of emission data during 10 minutes of scanning, the scanner's bed was translated by 3.4 mm (half of the slice thickness) and a second set of emission data was acquired, this resulted in two sets of 15 slices that were later interleaved. The absolute glucose consumption rate was calculated for each pixel using the Sokoloff equation [70]. In the quantification of metabolism a set of kinetic constants: K1 = 0.095, k2 = 0.125, k3 = 0.069, k4 = 0.055; and lumped constant (0.52) were used [71].

2.3. MRI studies

MRI studies were performed using one of two imaging systems. Thirty-five cases were scanned using a 1.5 T Phillips Gyroscan imager (Phillips International, Einhoven, The Netherlands) and three cases (from the MCI group) were scanned using a 1.5 T GE Advantage MR system (General Electric, Milwaukee, USA). Subjects' heads were positioned using a head holder and foam wedges. For both MRI scanners, five sagittal scout images were used to locate the long axis of the hippocampus and the coronal images were obtained perpendicular to that axis. Phillips scans, centered over the temporal lobes, consisted of eighteen 4 mm slices obtained with a T1-weighted spin-echo protocol (630/20/1/230 mm; TR/TE/excitations/FOV) and an acquisition matrix of 204 by 256 pixels. GE scans consisted of 124 T1-weighted 1.3 mm thick slices obtained with a 3D spoiled gradient recalled acquisition (SPGR) (35/9/1/180 mm/60°; TR/TE/excitations/FOV/flip angle) with an acquisition matrix of 256 by 128 pixels. To avoid measurement bias, prior to analysis, the GE scans were reformatted to match the resolution and slice profile of the Phillips scan.

2.4. Coregistration

The interleaved axial PET emission images were coregistered with the coronal MRI images on a Sun Sparc workstation (Sun Microsystems, Mountain View, California) using the Multimodal Image Data Analysis System (MIDAS) [72]. Brain parenchyma was separated from the scalp and skull [73] and an approximate image alignment was first done using the principal axes method [74]. Brain boundary points were extracted from the PET and MRI scans using an automatic edge finding algorithm, and the distance between the two surfaces was minimized using an iterative procedure. This resulted in the optimized values of 3 translational and 3 rotational parameters [75]. MRI was used as the target modality and the PET data was reformatted into the coronal orientation using trilinear interpolation methods. The final version of coregistered PET/MRI data consisted of eighteen 4 mm coronal sections with 230 mm FOV and 256 $\times$ 256 matrix. We previously estimated the coregistration error to be 1.3 mm [75].

2.5. Brain sampling

2.5.1. Regions of interest

Using gyral and sulcal landmarks, ROIs were reliably drawn [24] on three-fold enlarged coronal MRI images using MIDAS software by two observers who were blind to subject diagnosis. The ROIs, drawn on each MRI slice, could be visualized on the coregistered coronal PET images. Each of two observers drew all ROIs on half of the cases (randomly chosen). Each ROI was independently checked for accuracy by the other observer and any changes were made by joint agreement.

We sampled the hippocampus, parahippocampal gyrus, fusiform gyrus, the combined middle/inferior temporal gyri, and superior temporal gyrus. These regions were sampled anteriorly from the level of the anterior most amygdala and posteriorly to the level of the posterior pulvinar. This represents a rostral extension of our previously reported sampling boundaries [24,30,76]. To sample a region containing the entorhinal cortex (EC) the anterior portion of the parahippocampal gyrus was examined using boundaries derived from our post mortem validation study [41]. The anterior boundary for the anterior parahippocampal gyrus sample was 4 mm posterior to the fronto-temporal junction and the posterior boundary was the anterior margin of the lateral geniculate body. The superior boundary of the anterior parahippocampal gyrus in both anterior and posterior sections was the dorsal and most medial aspect of the parahippocampal gyrus. The inferior boundary was the collateral sulcus. In this paper we expand Amaral and Insausti's definition of the hippocampal formation [77] to include the white matter of the anterior parahippocampal gyrus in addition to the hippocampus proper, dentate gyrus, subicular complex and entorhinal cortex (see Fig. 1).

2.5.2. Normalization procedures

We sampled the MRglu at the center of a mid pontine slice at the level of the middle cerebral peduncles with a 54 $\times$ 22 mm box. The pons has been shown to have preserved glucose metabolism in AD [78,79] and was used to adjust for between-subject variations in the global MRglu [62,78,80–82]. The MRI volumes were corrected for variations in head size by using the volume of the intradural supratentorial compartment, which was outlined on all the slices containing ROIs [24].

2.5.3. CSF segmentation

Voxels containing CSF were identified from the regional samples. For each subject, the average MRI intensity of pure white matter in the temporal lobe multiplied by 0.55 yielded the upper threshold of CSF. In a phantom study, this constant was determined as the ratio of the intensity of white matter pixels to that of brain boundary pixels (composed of 50% gray matter and 50% CSF). Voxels that fell below this threshold for CSF were excluded from our MRI volumes.

2.5.4. MRglu correction for CSF (atrophy correction)

PET scans were corrected for the CSF partial volume effects employing a methodology similar to that proposed by Videen et al. [83], and implemented by Meltzer et al. [84,85] and Ibanez [86]. In short, the CSF was identified on every coronal slice using the above thresholding procedure and the MRI images were converted to binary images where pixels corresponding to brain were given a value of '1' and those corresponding to CSF were given a value of '0'. This binary image was convolved with the 3D point spread function of the CTI 931 PET camera. This resulted in a

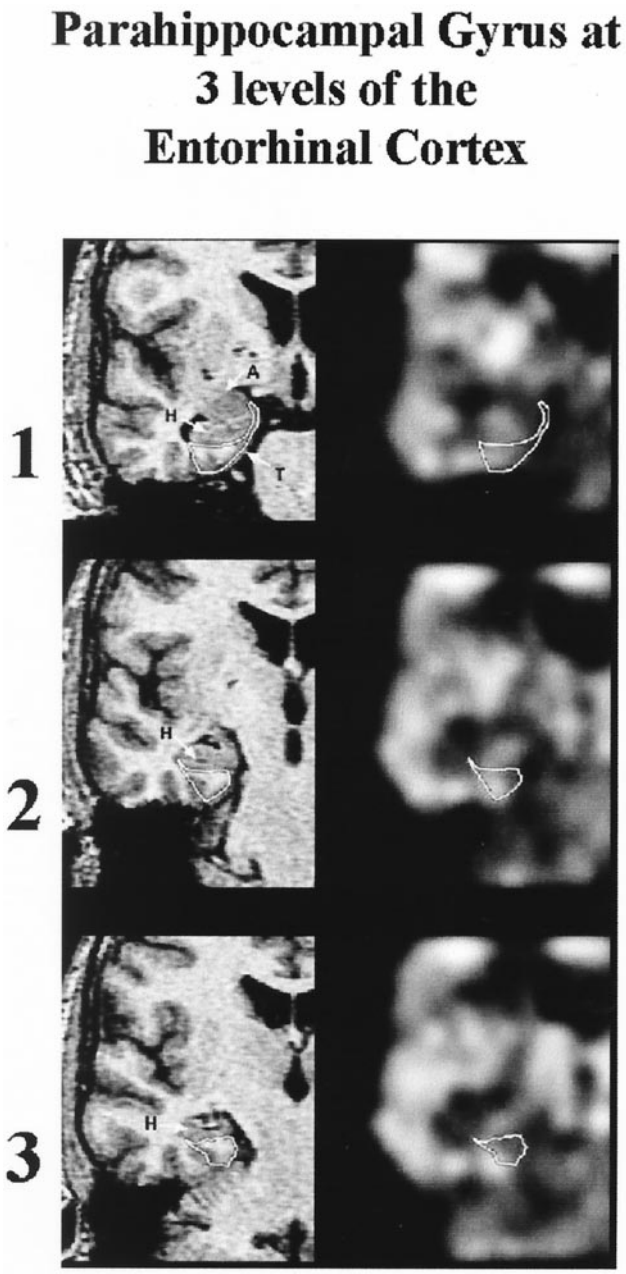

Fig. 1. Right parahippocampal gyrus ROI at 3 entorhinal cortex levels in a 63 year old male MCI patient. Arrows point to A = Amygdala, H = Hippocampus, T = Tentorium cerebelli.

recovery coefficient (RC) image. The coregistered PET image was divided by the RC image to yield a PET image corrected for atrophy. Atrophy corrected PET data was used in all statistical analyses. The corrections for atrophy raised the MRglu for the NL (range: 5–16%), MCI (range: 5–16%) and AD (range: 8–21%) groups.

2.6. PET validation procedures

Using patient data and simulated registration errors (1–4 mm in each plane) we computed for each ROI the effect of misregistration on the atrophy corrected metabolism. In appreciation of the decreasing size of the hippocampus posteriorly, we separately examined the larger anterior (pes) and posterior (body and tail) portions. We observed that the largest variations were seen in the posterior hippocampus with >8% change in MRglu when simulated registration errors were >2 mm. Consequently, we restricted the MRglu measurements of the hippocampus to the pes hippocampus region.

2.7. MRI validation procedures

For the three cases with GE MRI scans we degraded these scans to match the Phillips MRI scans by lowering the resolution and reformatting to the same orientation, pixel size, and slice thickness. To assess whether there was any bias imparted by this procedure, we examined the effect of MRI scan type on the regional MRglu and volume sampling for the one case that had both a Phillips and GE scan acquired at the time of the PET study. The PET scan was separately coregistered to both MRI scans. ROIs were independently drawn on each MRI scan to measure MRglu and volume. The results showed that the regional MRglu differences were less than 1.5%, and that there was good agreement between MRI machines (1% difference for the hippocampal volume and 3% difference for the volume of the superior temporal gyrus).

2.8. Hypotheses tested

1.) Hippocampal formation MRglu and volume measurements are superior to lateral neocortical measures in the discrimination of NL and MCI groups;
2.) Neocortical MRglu and volumetric measurements significantly add to hippocampal formation measures in the diagnosis of NL and AD, and MCI and AD groups;
3.) Regional MRglu measurements are diagnostically superior to the corresponding MRI volume measures.

3. Statistics and analyses

3.1.1. PET-MRglu calculation

For each region, across all slices sampled, the metabolic mean (μmole/100 g/min) weighted by the number of voxels was calculated.

3.1.2. MRI-volume calculations

The per slice average volume of each region was calculated by multiplying the number of sampled voxels by the voxel volume and dividing that product by the number of slices. This procedure, used in previous volume studies, reduces the bias when relatively thick slices are used and diseased groups have reduced numbers of slices [24].

3.1.3. Statistics

In an effort to reduce the number of variables tested, for both PET and MRI, mean values were averaged across hemispheres. One-way analyses of variance (ANOVAs) with appropriate follow-up tests were used to examine the demographic characteristics across groups. One-way analyses of covariance (ANCOVAs), controlling for age, gender, pontine metabolism or head size as confounds, were used to identify the significant regional metabolism or volume effects ($p < .05$) across the 3 clinical groups. Only statistically significant regions were used in logistic regression analyses to test the main hypotheses.

4. Results

4.1. Demographic characteristics

ANOVAs showed no group differences for age, education, and gender. Group differences were observed for the MMSE scores ($F [2,35] = 16.0$, $p < .001$). Post hoc comparisons between groups showed significantly lower MMSE scores for the AD group as compared to both the NL and MCI groups (p's $< .001$). The MMSE scores for the MCI and NL groups were not significantly different (see Table 1).

In the AD group we found that several PET and MRI regions correlated with age and gender. Therefore, we decided to take a conservative approach and in addition to the global metabolism (pons) and head size confounds, to control for age and gender in all subsequent analyses.

4.2. Omnibus and post hoc between group analyses

4.2.1. PET: between group regional differences

All regional PET ANCOVAs were found to be significantly different across the three groups after controlling for pontine metabolism, age, and gender (F's [2,32] ranged from 6.9 to 19.5, p's $< .05$). Follow up ANCOVAs for the paired groups showed that MCI relative to NL had significant ($p < .05$) MRglu reductions restricted to the hippocampus (10%), and the anterior parahippocampal gyrus (17%). For AD compared to NL, significant MRglu reductions were seen in all regions (ranging from 17% to 25%). In contrasting the MCI and AD groups, significant MRglu reductions (ranging from 10% to 18%) were found in AD for all temporal lobe regions except the anterior parahippocampal gyrus (8%, $p > .10$). (See Table 2 for unadjusted and covariate adjusted means and SD).

4.2.2. MRI: between group regional differences

ANCOVAs (controlling for head size, age and gender) showed a significant effect over all the 3 groups for only the hippocampus, middle/inferior temporal gyri and superior temporal gyrus. (F's [2,32] ranged from 3.3 to 8.8 with p's $< .05$). Follow up ANCOVAs for the paired groups (see Table 3 for unadjusted and covariate adjusted means and SD) showed a significant volume reduction restricted to the hippocampus (15%) for MCI relative to NL. AD cases showed significant volumetric reductions relative to NL in the hippocampus (19%), middle/inferior temporal gyri (10%), and superior temporal gyrus (10%). Contrasting MCI and AD, only the volume of the middle/inferior temporal gyri was significantly smaller in the AD group (8%).

Table 2
Atrophy corrected MRglu (μmole/100 g/min) unadjusted & **covariate adjusted**[1] means and standard deviations (SD)

	NL ($N = 11$)	MCI ($N = 15$)	AD ($N = 12$)
H	27.3 (4.1)	24.5 (3.3)	21.8 (4.5)
	27.4 (3.1)	**24.3 (3.1)**[a]	**21.9 (3.1)**[a,c]
Ant. PHG	28.8 (3.5)	23.9 (3.7)	21.9 (3.7)
	28.7 (3.2)	**23.8 (3.2)**[b]	**21.9 (3.2)**[b]
Post. PHG	31.4 (4.4)	29.1 (4.2)	25.0 (4.5)
	31.5 (3.6)	**28.9 (3.7)**	**25.1 (3.6)**[b,d]
FG	31.7 (3.5)	29.6 (4.2)	25.4 (5.4)
	31.8 (4.1)	**29.4 (4.1)**	**25.6 (4.0)**[b,c]
MITG	32.0 (4.1)	28.9 (4.5)	23.7 (3.3)
	31.7 (3.1)	**28.9 (3.1)**	**23.8 (3.1)**[b,d]
STG	34.9 (4.1)	32.0 (3.9)	28.7 (2.9)
	34.7 (2.8)	**32.0 (2.8)**	**28.8 (2.8)**[b,d]
Pons	22.8 (2.9)	22.3 (4.1)	22.4 (3.0)

[1] Adjusted for pontine MRglu, age, and gender.
[a] Significantly different from NL ($p \leq .05$).
[b] Significantly different from NL ($p \leq .01$).
[c] Significantly different from MCI ($p \leq .05$).
[d] Significantly different from MCI ($p \leq .01$).
H = hippocampus, Ant PHG = anterior parahippocampal gyrus, Post PHG = posterior parahippocampal gyrus, FG = fusiform gyrus, MITG = middle/inferior temporal gyrus, STG = superior temporal gyrus.

Table 3
Unadjusted & **covariate adjusted**[1] regional mean volumes (cc's) and standard deviations (SD)

	NL (N = 11)	MCI (N = 15)	AD (N = 12)
H	1.26 (0.17)	1.07 (0.14)	0.98 (0.13)
	1.25 (0.16)	**1.06 (0.12)**[b]	**1.01 (0.11)**[b]
Ant. PHG	2.36 (0.43)	2.24 (0.49)	1.91 (0.50)
	2.35 (0.48)	**2.21 (0.50)**	**1.95 (0.50)**
Post. PHG	1.97 (0.32)	1.74 (0.26)	1.62 (0.25)
	1.90 (0.26)	**1.73 (0.25)**	**1.70 (0.22)**
FG	2.24 (0.45)	2.15 (0.51)	1.83 (0.38)
	2.18 (0.42)	**2.13 (0.37)**	**1.92 (0.39)**
MITG	7.92 (1.07)	7.40 (0.95)	6.84 (1.12)
	7.57 (0.74)	**7.38 (0.68)**	**6.82 (0.72)**[a,c]
STG	5.96 (0.76)	5.36 (0.74)	4.88 (0.57)
	5.71 (0.53)	**5.38 (0.50)**	**5.12 (0.50)**[a]
Head size	85.6 (6.32)	82.4 (6.44)	79.2 (6.40)

[1] Adjusted for head size, age, and gender.
[a] Significantly different from NL ($p \leq .05$).
[b] Significantly different from NL ($p \leq .01$).
[c] Significantly different from MCI ($p \leq .05$).
H = hippocampus, Ant PHG = anterior parahippocampal gyrus, Post. PHG = posterior parahippocampal gyrus, FG = fusiform gyrus, MITG = middle/inferior temporal gyrus, STG = superior temporal gyrus.

Table 4
Diagnostic classification accuracies for PET and MRI

Region	NL and MCI		MCI and AD		NL and AD	
	PET	MRI	PET	MRI	PET	MRI
H	73%[a]	73%[b]	70%[a]		91%[b]	83%[b]
Ant. PHG	85%[b]				96%[b]	
Post. PHG			63%[b]		91%[b]	
FG			67%[a]		87%[b]	
MITG			81%[b]	81%[a]	100%[b]	78%[a]
STG			70%[b]		100%[b]	78%[b]

[a] $p < .05$.
[b] $p < .01$.
H = hippocampus, Ant. PHG = anterior parahippocampal gyrus, Post PHG = posterior parahippocampal gyrus, FG = fusiform gyrus, MITG = middle/inferior temporal gyrus, STG = superior temporal gyrus.

4.3. Within modality diagnostic accuracy: tests of hypotheses 1 and 2

Separately for PET and MRI, two types of hierarchical logistic regression analyses were used to derive group classification data. First, we obtained the between group classifications for each significant region from the omnibus ANCOVAs. This was done by entering the confounds in step one and the region as step two. Secondly, we determined the unique variance for each region after accounting for all other regions. In these analyses we entered the confounds and all but one region as the first step. In the second step we entered the one region to be tested.

4.3.1. NL and MCI classification

MCI patients showed predominant hippocampal formation changes that are detected with both PET and MRI.

4.3.1.1. PET MRglu. The ANCOVAs showed that two regions, the anterior parahippocampal gyrus and the hippocampus had significantly lower MRglu in the MCI group compared to NL. The logistic regression analyses showed that the anterior parahippocampal gyrus MRglu correctly classified 85% of the NL and MCI patients (82% NL, 87% MCI). The hippocampus MRglu classified 73% of these cases (see Table 4). Moreover, only the anterior parahippocampal gyrus when entered as the second step (after the confounds and the hippocampus), significantly contributed to the regression model resulting in an overall classification of 81% (82% NL and 80% MCI; χ^2_{change} (1) = 8.4, $p < .01$).

4.3.1.2. MRI region volume. The hippocampal volume when entered into the logistic regression model after the confounds reached a significant overall classification of 73% (64% NL and 80% MCI groups; χ^2_{change} (1) = 10.8, $p = .001$). Since the hippocampus was the only region that significantly separated NL from MCI groups, no comparisons to assess the uniqueness of this finding were conducted (see Table 4).

4.3.2. NL and AD classification

AD patients when compared to NL showed widespread metabolic and volumetric reductions involving the hippocampal formation and the temporal neocortical areas.

4.3.2.1. PET MRglu. All six temporal lobe regions had significantly lower metabolic values for the AD group compared to the NL group in the ANCOVAs. Based on the individual region regression analyses (see Table 4) the middle/inferior temporal gyrus and the superior temporal gyrus were both ideal group discriminators, each classifying 100% of the NL and AD groups (χ^2_{change} (1) = 31.6, $p < .0001$ for both regions). Consequently, the unique variance contributed by other regions could not be evaluated.

4.3.2.2. MRI region volume. The ANCOVAs showed that three temporal lobe regional volumes (hippocampus, middle/inferior temporal gyri, and superior temporal gyrus) were significantly smaller in AD compared to NL. Of these, the logistic regression analyses showed that the hippocampal volume produced the highest overall classification accuracy (83%) (see Table 4). In the second logistic regression model, none of the three regions uniquely contributed to the explained variance over the other regions. In each case, 100% classification was reached at the second regression step.

4.3.3. MCI and AD classification

In the classification of MCI and AD metabolic and volumetric measures of the middle and inferior temporal gyri were superior.

4.3.3.1. PET MRglu. The ANCOVAs showed that all temporal lobe regions except the anterior parahippocampal gyrus were significant. From the regional logistic regression analyses, we found overall group classifications ranging from 63%–81% (see Table 4) with the middle/inferior temporal gyrus achieving the best overall group classification (81%). In the second logistic regression model two regions, the fusiform gyrus (χ^2_{change} (1) = 5.6, $p < .05$) and the middle/inferior temporal gyri (χ^2_{change} (1) = 8.7, $p < .01$), when added as the second step, significantly added to the classification accuracy. For both regions the classification was the same (85% overall; 80% MCI, 92% AD). Given that as individual regions the middle/inferior temporal gyri classified 81% of the MCI and AD groups and the fusiform gyrus only classified 67%, we conclude that middle/inferior gyri is superior in the diagnosis of MCI and AD.

4.3.3.2. MRI region volume. Only the middle/inferior temporal gyri sample was significantly different between the MCI and the AD groups in the ANCOVA. Consequently, only the first logistic regression model was examined. The results showed that when middle/inferior temporal gyri was entered after the confounds, 81% were classified correctly (87% MCI, 75% AD groups; χ^2_{change} (1) = 5.7, $p < .05$).

4.4. Regional comparisons between imaging modalities: test of hypothesis 3

The individual regions significantly separating the pairs of groups studied above were tested using a 3-step logistic regression analysis model to determine whether the PET-MRI measure added to the volume in the classification of subjects between diagnostic groups. In the first step, confounds for both modalities (head size, metabolism of the pons, age, and gender) were entered. In the second step, the region volume was entered, and in the third step, the corresponding regional MRglu was entered. By inverting steps 2 and 3 in the above model we also examined the contribution of volume above metabolism.

For NL and MCI groups the anterior parahippocampal gyrus MRglu significantly increased the number of cases correctly classified by volume from 78% to 88% (χ^2_{change} (1) = 13.4, $p < .001$). However, the hippocampal MRglu, did not add to volume in classifying the groups.

For NL and AD groups, 100% classification was achieved in each regression model with the separate entry at the third step of MRglu of the anterior parahippocampal, fusiform, middle/inferior temporal, and superior temporal gyri, which was a significant improvement beyond their volumes (74%, 78%, and 83% respectively, $\chi^2_{\text{change's}}$ (1) range from 16.7 to 21.3, p's $< .0001$). The overall classification accuracy for both the hippocampus and posterior parahippocampal gyrus MRglu was 91%. This represented an increase beyond the volume-based classification of 83% (χ^2_{change} (1) = 5.0, $p < .05$) and 78% (χ^2_{change} (1) = 9.9, $p < .01$) respectively.

For the MCI and AD groups the MRglu significantly improved the classification above the volume in all regions (χ^2_{change} (1) range from 4.5 to 15.0, p's $< .05$): the hippocampus improved from 52% to 70%, fusiform gyrus 59% to 63%, middle/inferior temporal gyri 82% to 89%, posterior parahippocampal gyrus 48% to 74% and superior temporal gyrus 63% to 74%.

After inverting steps 2 and 3 in the above models none of the volumes added to the MRglu in the group classifications.

Generally, the best regional PET classifier was also the best MRI classifier (see Table 4). However, in the NL and MCI discrimination the anterior parahippocampal gyrus was the best PET classifier (81%) and the hippocampal volume was the best MRI classifier (73%). In a model contrasting the anterior parahippocampal metabolism and hippocampal volume, we found that when either variable was entered as the third step, 100% classification was achieved. This result suggests the equivalence of these measures in the classification of NL and MCI.

In summary, for the three pair-wise group comparisons glucose metabolism measures were generally superior to volume measures in diagnostic group classifications.

5. Discussion

5.1. The diagnosis of MCI

Our most important finding is that only hippocampal formation regions for both PET and MRI clearly separated NL and MCI subjects. We observed that the glucose utilization of the anterior parahippocampal gyrus and the hippocampus were the superior PET diagnostic measures and the best MRI measure was the volume of the hippocampus.

We believe that these PET results are the first to demonstrate reductions in MRglu of the anterior parahippocampal gyrus and hippocampus in MCI. Based on our previous validation work [41] we are confident that this anterior parahippocampal region includes the EC region. A prior FDG-PET study reported that very mild AD patients (CDR 0.5) did not show reduced parahippocampal gyrus MRglu [62]. This group did not distinguish the EC region from a larger parahippocampal gyrus sample which may have contributed to this negative finding.

The MRI component of the present study is consistent with many other MRI studies that have shown the hippocampus to be useful in the diagnosis of MCI [28,29,38, 87]. This work also replicates our previous MRI findings by demonstrating, relative to other temporal lobe sub-regions, the anatomic specificity of hippocampal atrophy in MCI [24].

Only recently have MRI studies examined entorhinal cortex size [31,40,88]. These studies show that EC size is of value in the diagnosis of AD [41,88] and MCI [31]. The present study did not find a significant volume change in the anterior parahippocampal gyrus in MCI. However, this negative finding is not surprising as our study sampled the entire volume of the anterior parahippocampal gyrus (including the white matter), and as such, was not comparable to studies that targeted only the gray matter.

For the PET for the anterior parahippocampal gyrus was superior to the hippocampus in discriminating between NL and MCI individuals. However across modalities the hippocampus was the most consistent brain region in the diagnosis of NL and MCI. When comparing the MRglu of the anterior parahippocampal gyrus and volume of the hippocampus, both regions were equally good at classifying the groups. This suggests that regional PET and MRI assessments of hippocampal formation structures add uniquely to the diagnosis and description of MCI.

These cross-sectional observations of MCI patients require longitudinal follow-up to confirm their predictive value for future cognitive decline to AD. One longitudinal PET case study has been reported but the hippocampal metabolism was not examined [58]. Among PET prediction studies none examined the hippocampus [63,89]. Some of these, however, did find lateral temporal lobe and posterior cingulate gyrus changes.

Several structural imaging studies of MCI patients designed to identify either longitudinal brain change or predict

longitudinal behavioral change report baseline parahippocampal gyrus [29], hippocampal [22,25–27] and temporal neocortical [25,30,31] size reductions in individuals who decline to AD compared to those who remain stable. Using both PET and MRI in a longitudinal design may provide improved diagnostic sensitivity.

5.2. The diagnosis of AD

Our second finding is that in the classification of NL and AD, and of MCI and AD there are significant MRglu and volumetric reductions in both the hippocampal formation and in the neocortex of AD patients. However, the neocortical sites typically yielded greater diagnostic accuracy, thus confirming hypothesis 2.

While we, and others, have reported hippocampal MRglu reductions in mild AD [50–54], some studies did not observe hippocampal hypometabolism in AD [55–57]. These negative studies are likely due to PET sampling in the absence of coregistered MRI or sampling the hippocampus without considering the relationships between structure size and shape and isotope recovery. We attempted to maximize isotope recovery in this study by using double-sampling of the PET data. Hippocampal volume reductions have been consistently reported in AD [26,35–38,90,91] and this was our best individual regional volumetric classifier for NL and AD groups.

We found that across both imaging modalities the most consistent discriminator of AD from the NL and the MCI groups was the middle/inferior temporal gyri. This finding is consistent with neuropathological observations that also imply that the progression to dementia is reflected in the involvement of the temporal lobe neocortex [6,9,92,93]. Our data are also consistent with the longstanding observations from the PET and MRI literatures that highlight lateral temporal lobe deficits in AD (see [30,35,90,94] and [95] for review).

We did not find volume reductions of the fusiform gyrus in AD subjects compared to MCI, which we had previously reported [24]. The present study extended the anterior most slice from the level of the posterior pes hippocampus to the level of the anterior limit of the amygdala. It appears that this change accounts for the discrepant results. Examining the fusiform volume using our previously reported boundaries [24], we found a significant group main effect ($F[2,32] = 3.4$, $p = .05$). Follow-up ANCOVA's showed significant size reductions in the AD group relative to the NL group ($F[1,1,18] = 5.1$, $p < .05$) and to the MCI group ($F[1,22] = 6.2$, $p < .05$). At present we have no satisfactory neuropathological or anatomical explanation for this boundary related observation. Possibly the discrepancy is due to the previously reported increased anatomical variation of the anterior medial and lateral occipitotemporal sulcal boundaries for the fusiform gyrus [96]. Examining the coefficient of variation in the normal group we found greater variability in the anterior versus posterior fusiform gyrus (27% and 19% respectively). In this study we did not examine the parietal area as our PET and MRI coverage did not extend superior and posterior enough to ensure adequate sampling in all cases.

Overall these PET and MRI data support the neuropathological view of Braak and Braak [6] that AD brain changes can be seen as stages of neurofibrillary pathology, beginning in the medial temporal lobe and ultimately spreading to the lateral temporal lobe neocortex and other sites. Both our PET and MRI results identify the hippocampal formation as the most informative region in the discrimination of NL and MCI. This suggests the potential for identifying an early stage of brain involvement. With AD, neocortical sites are the better classifiers, thus indicating a later stage of more widespread brain involvement.

5.3. Cross modality comparisons

We found that PET MRglu measures are for the most part better at patient classification than MRI volume measures. Our data show that after controlling for structure size, the MRglu measurement significantly contributes to the diagnostic accuracy. One exception was noted in the NL and MCI classification where the volume of the hippocampus was as good as the MRglu of the hippocampus in the classification. For the hippocampus both PET and MRI contribute uniquely to the diagnosis and characterization of MCI and NL. In conclusion, given that two PET regions and only one MRI region significantly separated NL and MCI and that the MRglu of the anterior parahippocampal gyrus had a higher overall classification accuracy than did hippocampal volume, we conclude that MRglu measures are the superior classifiers of group membership for all pairwise group contrasts. Longitudinal studies are required to determine whether changes in metabolism can be detected prior to changes in volume.

5.4. Limitations

Neuropathological studies show a predominant loss of gray matter in AD [97,98]. Previously, using MRI with inversion recovery sequences, we identified a 14% loss of gray matter and a 2% loss in white matter in the temporal lobes of AD subjects compared to elderly controls [99]. The atrophy correction model we used [83,84] does not account for the disease related changes in the relative volume of the gray and white matter. In the current study we were unable to accurately separate gray from white matter with the available MRI pulse sequences. Consequently, there may be different proportions of gray matter in the volumes across groups. Depending on the magnitude of the gray matter volume loss and the health of the metabolically active gray matter remaining we may be under or overestimating the regional MRglu.

6. Conclusion

These cross-sectional neuroimaging data offer support for the idea that AD pathology is earliest seen in the hippocampal formation and subsequently there is involvement of the temporal lobe neocortex. Specifically, MRglu and volume losses in hippocampal formation regions best characterize MCI patients while evidence for additional neocortical damage best characterizes AD patients. Further, as these data indicate the superior diagnostic sensitivity of PET over MRI, they suggest continued MRglu study of the course and treatment of AD.

Acknowledgments

This study was supported by NIH/NIA grants AG 13616, AG 08051 and AG 12101.

We wish to thank Dr. Elia Sinaiko for his statistical review of this document. We also thank Donald Warner, Robert Carciello for PET and cyclotron operations, Noelwah Netusil and Pauline Carter for subject care during the PET procedure, and Richard Ferrieri, David Alexoff, Colleen Shea and Robert MacGregor for FDG synthesis.

References

[1] Tomlinson BE, Blessed G, Roth M. Observations on the brains of non-demented old people. Journal of Neurological Sciences 1968; 7:331–56.
[2] Kemper T. Neuroanatomical and neuropathological changes in normal aging and in dementia. In: Albert ML, editor. Clinical Neurology of Aging. New York: Oxford University Press, 1984. pp. 3–67.
[3] Ulrich J. Alzheimer changes in nondemented patients younger than sixty-five: possible early stages of Alzheimer's disease and senile dementia of Alzheimer type. Ann Neurol 1985;17:273–7.
[4] Hubbard BM, Fenton GW, Anderson JM. A quantitative histological study of early clinical and preclinical Alzheimer's disease. Neuropathology and Applied Neurobiology 1990;16:111–21.
[5] Braak H, Braak E. Neurofibrillary changes confined to the entorhinal region and an abundance of cortical amyloid in cases of presenile and senile dementia. Acta Neuropathologica 1990;80:479–86.
[6] Braak H, Braak E. Neuropathological stageing of Alzheimer-related changes. Acta Neuropathologica 1991;82:239–59.
[7] Arriagada PV, Marzloff K, Hyman BT. Distribution of Alzheimer-type pathologic changes in nondemented elderly individuals matches the pattern in Alzheimer's disease. Neurol 1992;42:1681–8.
[8] Langui D, Probst A, Ulrich J. Alzheimer's changes in non-demented and demented patients: a statistical approach to their relationships. Acta Neuropathology 1995;89:57–62.
[9] Giannakopoulos P, Hof PR. Distinct patterns of neural loss and Alzheimer's disease lesion distribution in elderly individuals older than 90 years. J Neuropath Exp Neurol 1996;55:1210–20.
[10] Gomez-Isla T, Price JL, McKeel DW, Morris JC, Growdon JH, Hyman BT. Profound loss of layer II entorhinal cortex neurons occurs in very mild Alzheimer's disease. The Journal of Neuroscience 1996;16:4491–4500.
[11] Ghebremedhin E, Schultz C, Braak E, Braak H. High frequency of apolipoprotein E ϵ4 allele in young individuals with very mild Alzheimer's disease-related neurofibrillary changes. Exp Neurol 1998;153:152–5.
[12] Price JL, Morris JC. Tangles and plaques in nondemented aging and "preclinical" Alzheimer's disease. Ann Neurol 1999;45:358–68.
[13] Price JL, Davis PB, Morris JC, White DL. The distribution of tangles, plaques and related immunohistochemical markers in healthy aging and Alzheimer's disease. Neurobiology of Aging 1991;12:295–312.
[14] Johansson K, Bogdanovic N, Kalimo H, Winblad B, Viitanen M. Alzheimer's disease and apolipoprotein E ϵ4 allele in older drivers who died in automobile accidents. Lancet 1997;349:1143–4.
[15] Mufson EJ, Chen E-Y. Entorhinal cortex beta-amyloid load in individuals with mild cognitive impairment. Exp Neurol 1999;158: 469–90.
[16] Hof PR, Cox K, Morrison JH. Quantitative analysis of a vulnerable subset of pyramidal neurons in Alzheimer's disease: I. Superior frontal and inferior temporal cortex. The Journal of Comparative Neurology 1990;301:44–54.
[17] Mann DMA. The topographic distribution of brain atrophy in Alzheimer's disease. Acta Neuropathologica 1991;83:81–6.
[18] Berg L, McKeel DW, Miller JP, Baty J, Morris JC. Neuropathological indexes of Alzheimer's disease in demented and nondemented persons aged 80 years and older. Arch Neurol 1993;50:349–58.
[19] Dawe B, Procter A, Philpot M. Concepts of mild memory impairment in the elderly and their relationship to dementia—a review. International Journal of Psychophysiology 1992;7:473–9.
[20] Flicker C, Ferris SH, Reisberg B. Mild cognitive impairment in the elderly: predictors of dementia. Neurol 1991;41:1006–9.
[21] Petersen RC, Smith GE, Waring SC, Ivnik RJ, Tangalos EG, Kokmen E. Mild cognitive impairment: clinical characterization and outcome. Arch Neurol 1999;56:303–8.
[22] de Leon MJ, George AE, Stylopoulos LA, Smith G, Miller DC. Early marker for Alzheimer's disease: the atrophic hippocampus. Lancet 1989;2:672–3.
[23] Scheltens P, Leys D, Barkhof F, Huglo D, Weinstein HC, Vermersch P, Kuiper M, Steinling M, Wolters EC, Valk J. Atrophy of medial temporal lobes on MRI in "probable" Alzheimer's disease and normal aging: diagnostic value and neuropsychological correlates. J Neurol Neurosurg Psychiatry 1992;55:967–72.
[24] Convit A, de Leon MJ, Tarshish C, De Santi S, Tsui W, Rusinek H, George AE. Specific hippocampal volume reductions in individuals at risk for Alzheimer's disease. Neurobiology of Aging 1997;18: 131–8.
[25] Kaye JA, Swihart T, Howieson D, Dame A, Moore MM, Karnos T, Camicioli R, Ball M, Oken B, Sexton G. Volume loss of the hippocampus and temporal lobe in healthy elderly persons destined to develop dementia. Neurol 1997;48:1297–304.
[26] de Leon MJ, Golomb J, George AE, Convit A, Tarshish CY, McRae T, De Santi S, Smith G, Ferris SH, Noz M, Rusinek H. The radiologic prediction of Alzheimer's disease: the atrophic hippocampal formation. American Journal of Neuroradiology 1993;14: 897–906.
[27] Jack CR, Petersen RC, Xu YC, O'Brien PC, Smith GE, Ivnik RJ, Boeve BF, Waring SC, Tangalos EG, Kokmen E. Prediction of AD with MRI-based hippocampal volume in mild cognitive impairment. Neurol 1999;52:1397–403.
[28] Fox NC, Warrington EK, Freeborough PA, Hartikainen P, Kennedy AM, Stevens JM, Rossor MN. Presymptomatic hippocampal atrophy in Alzheimer's disease: a longitudinal MRI study. Brain 1996; 119:2001–7.
[29] Visser PJ, Scheltens P, Verby FRJ, Schmand B, Launer LJ, Jolles J, Jonker C. Medial temporal lobe atrophy and memory dysfunction as predictors for dementia in subjects with mild cognitive impairment. J Neurol 1999;246:477–85.
[30] Convit A, de Asis J, de Leon MJ, Tarshish C, De Santi S, Rusinek H. Atrophy of the Medial Occipitotemporal, Inferior, and Middle Temporal Gyri in non-demented elderly predict decline to Alzheimer's disease. Neurobiology of Aging 2000;21:19–26.

[31] Killiany RJ, Gomez-Isla T, Moss M, Kikinis R, Sandor T, Jolesz F, Tanzi R, Jones K, Hyman B, Albert MS. Use of structural magnetic resonance imaging to predict who will get Alzheimer's disease. Ann Neurol 2000;47:430–9.
[32] de Leon MJ, George AE, Reisberg B, Ferris SH, Kluger A, Stylopoulos LA, Miller JD, La Regina ME, Chen C, Cohen J. Alzheimer's disease: longitudinal CT studies of ventricular change. American Journal of Neuroradiology 1989;10:371–6.
[33] Xanthakos S, Ranga Rama Krishnan K, Kim DM, Charles HC. Magnetic resonance imaging of Alzheimer's disease. Prog Neuro-Psychopharmacol & Biol Psychiat 1996;20:597–626.
[34] Kesslak JP, Nalcioglu O, Cotman CW. Quantification of magnetic resonance scans for hippocampal and parahippocampal atrophy in Alzheimer's disease. Neurol 1991;41:51–4.
[35] Killiany RJ, Moss MB, Albert MS, Sandor T, Tieman J, Jolesz F. Temporal lobe regions on magnetic resonance imaging identify patients with early Alzheimer's disease. Arch Neurol 1993;50:949–54.
[36] Jack CR, Petersen RC, O'Brien PC, Tangalos EG. MR-based hippocampal volumetry in the diagnosis of Alzheimer's disease. Neurol 1992;42:183–8.
[37] Krasuski JS, Alexander GE, Horwitz B, Daly EM, Murphy D, Rapoport SI, Schapiro MB. Volumes of medial temporal lobe structures in patients with Alzheimer's disease and mild cognitive impairment (and in healthy controls). Biological Psychiatry 1998;43:60–8.
[38] Jack CR, Petersen RC, Xu YC, Waring SC, O'Brien PC, Tangalos EG, Smith GE, Ivnik RJ, Kokmen E. Medial temporal atrophy on MRI in normal aging and very mild Alzheimer's disease. Neurol 1997;49:786–94.
[39] Laakso MP, Soininen H, Partanen K, Lehtovirta M, Hallikainen M, Hanninen T, Helkala E-L, Vainio P, Riekkinen PJ. MRI of the hippocampus in Alzheimer's disease: sensitivity, specificity, and analysis of the incorrectly classified subjects. Neurobiology of Aging 1998;19:23–31.
[40] Juottonen K, Laakso MP, Partanen K, Soininen H. Comparative MR Analysis of the entorhinal cortex and hippocampus in diagnosing Alzheimer disease. American Journal of Neuroradiology 1999;20:139–44.
[41] Bobinski M, de Leon MJ, Convit A, De Santi S, Wegiel J, Tarshish CY, Saint-Louis LA, Wisniewski HH. MRI of entorhinal cortex in mild Alzheimer's disease. Lancet 1999;353:38–40.
[42] Xu Y, Jack CRJ, O'Brien PC, Kokmen E, Smith GE, Ivnik RJ, Boeve BF, Tangalos RG, Petersen RC. Usefulness of MRI measures of entorhinal cortex versus hippocampus in AD. Neurol 2000;54:1760–7.
[43] Friedland RP, Budinger TF, Ganz E, Yano Y, Mathis CA, Koss B, Ober BA, Huesman RH, Derenzo SE. Regional cerebral metabolic alterations in dementia of the Alzheimer type: positron emission tomography with [18F] fluorodeoxyglucose. Journal of Computer Assisted Tomography 1983;7:590–8.
[44] Foster NL, Chase TN, Mansi L, Brooks R, Fedio P, Patronas NJ, Di Chiro G. Cortical abnormalities in Alzheimer's disease. Ann Neurol 1984;16:649–54.
[45] Duara R, Grady C, Haxby J, Sundaram M, Cutler NR, Heston L, Moore A, Schlageter N, Larson S, Rapoport SI. Positron emission tomography in Alzheimer's disease. Neurol 1986;36:879–87.
[46] Small GW, Kuhl DE, Riege WH, Fujikawa DG, Ashford JW, Metter EJ, Mazziotta JC. Cerebral glucose metabolic patterns in Alzheimer's disease. Effect of gender and age at dementia onset. Arch Gen Psychiat 1989;46:527–32.
[47] Kumar A, Schapiro MB, Grady C, Haxby JV, Wagner E, Salerno JA, Friedland RP, Rapoport SI. High-resolution PET studies in Alzheimer's disease. Neuropsychopharmacology 1991;4:35–46.
[48] Jagust WJ, Friedland RP, Budinger TF, Koss E, Ober B. Longitudinal studies of regional cerebral metabolism in Alzheimer's disease. Neurol 1988;38:909–12.
[49] Smith GS, de Leon MJ, George AE, Kluger A, Volkow ND, McRae T, Golomb J, Ferris SH, Reisberg B, Ciaravino J, La Regina MA. Topography of cross-sectional and longitudinal glucose metabolic deficits in Alzheimer's disease: pathophysiologic implications. Arch Neurol 1992;49:1142–50.
[50] Perani D, Bressi S, Cappa SF, Vallar G, Alberoni M, Grassi F, Caltagirone C, Cipolotti L, Franceschi M, Lenzi GL, Fazio F. Evidence of multiple memory systems in the human brain: a [18F]FDG PET metabolic study. Brain 1993;116:903–19.
[51] de Leon MJ, McRae T, Rusinek H, Convit A, De Santi S, Tarshish C, Golomb J, Volkow N, Daisley K, Orentreich N, McEwen B. Cortisol reduces hippocampal glucose metabolism in normal elderly but not in Alzheimer's disease. Journal of Clinical Endocrinology and Metabolism 1997;82:3251–9.
[52] Ouchi Y, Nobezawa S, Okada H, Yoshikawa E, Futatsubashi M, Kaneko M. Altered glucose metabolism in the hippocampal head in memory impairment. Neurol 1998;51:136–42.
[53] Stein DJ, Buchsbaum MS, Hof PR, Siegel BV, Shihabuddin L. Greater metabolic rate decreases in hippocampal formation and proisocortex than in neocortex in Alzheimer's disease. Neuropsychobiology 1998;37:10–9.
[54] Desgranges B, Baron J-C, De La Sayette V, Petit-Taboue MC, Benali K, Landeau B, Lechevalier B, Eustache F. The neural substrates of memory systems impairment in Alzheimer's disease a PET study of resting brain glucose utilization. Brain 1998;121:611–31.
[55] Fukuyama H, Harada K, Yamauchi H, Miyoshi T, Yamaguchi S, Kimura J, Kameyama M, Senda M, Yonekura Y, Konishi J. Coronal reconstruction images of glucose metabolism in Alzheimer's disease. Journal of the Neurological Sciences 1991;106:128–34.
[56] Jagust WJ, Eberling JL, Richardson BC, Reed BR, Baker MG, Nordahl TE, Budinger TF. The cortical topography of temporal lobe hypometabolism in early Alzheimer's disease. Brain Res 1993;629:189–98.
[57] Ishii K, Sasaki M, Yamaji S, Sakamoto S, Kitagaki H, Mori E. Relatively preserved hippocampal glucose metabolism in mild Alzheimer's disease. Dementia and Geriatric Cognitive Disorders 1998;9:317–22.
[58] Pietrini P, Azari NP, Grady CL, Salerno JA, Gonzalez-Aviles A, Heston LL, Pettigrew KD, Horwitz B, Haxby JV, Schapiro MB. Pattern of cerebral metabolic interactions in a subject with isolated amnesia at risk for Alzheimer's disease: a longitudinal evaluation. Dementia 1993;4(2):94–101.
[59] Small GW, Okonek A, Mandelkern MA, LaRue A, Chang L, Khonsary A, Ropchan JR, Blahd WH. Age-associated memory loss: initial neuropsychological and cerebral metabolic findings of a longitudinal study. Int Psychogeriat 1994;6:23–44.
[60] Small GW, Mazziotta JC, Collins MT, Baxter LR, Phelps ME, Mandelkern MA, Kaplan A, LaRue A, Adamson CF, Chang L, Guze BH, Corder EH, Saunders AM, Haines JL, Pericak-Vance MA, Roses AD. Apolipoprotein E type 4 allele and cerebral glucose metabolism in relatives at risk for familial Alzheimer disease. JAMA 1995;273:942–7.
[61] De Santi S, de Leon MJ, Rusinek H, Golomb J, Convit A, Tarshish C, McRae T, Kluger A, Fowler J, Volkow N, Wolf AP. Selective medial temporal lobe pathology in cases at-risk for AD: diagnostic role of PET. In: Iqbal K, Mortimer J, Winblad B, Wisniewski H, editors. Research advances in Alzheimer's disease and related disorders, Sussex, England: John Wiley & Sons, Ltd., 1995. pp. 173–80.
[62] Minoshima S, Giordani B, Berent S, Frey KA, Foster NL, Kuhl DE. Metabolic reduction in the posterior cingulate cortex in very early Alzheimer's disease. Ann Neurol 1997;42:85–94.
[63] Berent S, Giordani B, Foster N, Minoshima S, Lajiness-O'Neill R, Koeppe R, Kuhl DE. Neuropsychological function and cerebral glucose utilization in isolated memory impairment and Alzheimer's disease. J Psychiat Res 1999;33:7–16.

[64] Reisberg B, Ferris SH, de Leon MJ, Crook T. The global deterioration scale for assessment of primary degenerative dementia. Am J Psychiat 1982;139:1136–9.
[65] Folstein M. The Mini-Mental State Examination. In: Crook T, Ferris SH, Bartus R, editors. Assessment in Geriatric Psychopharmacology. New Canaan: Mark Powley Associates, 1983. pp. 47–51.
[66] McKhann G, Drachman D, Folstein M, Katzman R, Price D, Stadlan EM. Clinical diagnosis of Alzheimer's disease: report of the NINCDS-ADRDA work group under the auspices of Department of Health & Human Services Task Force on Alzheimer's disease. Neurol 1984;34:939–44.
[67] American Psychiatric Association, Diagnostic and Statistical Manual of Mental Disorders (Fourth Edition), American Psychiatric Association, Washington, D.C., 1994.
[68] de Leon MJ, Golomb J, George AE, Convit A, Rusinek H, Morys J, Bobinski M, De Santi S, Tarshish C, Narkiewicz O, Wisniewski HM. Hippocampal formation atrophy in aging and the prediction of Alzheimer's disease. In: Burns A, editor. Ageing and dementia: a methodological approach. London: Edward Arnold, 1993. pp. 103–24.
[69] Kluger A, Ferris SH, Golomb J, Mittelman MS, Reisberg B. Neuropsychological prediction of decline to dementia in nondemented elderly. J Geriat Psychiat Neurol 1999;12:168–79.
[70] Sokoloff L, Reivich M, Kennedy C, Des Rosiers MH, Patlak CS, Pettigrew KD, Sakurada O, Shinohara M. The [14C]deoxyglucose method for the measurement of local cerebral glucose utilization: theory, procedure, and normal values in the conscious and anesthetized albino rat. J Neurochem 1977;28:897–916.
[71] Reivich M, Alavi A, Wolf A, Fowler J, Russell J, Arnett C, MacGregor RR, Shiue CY, Atkins H, Anand A, Dann R, Greenberg J. Glucose metabolic rate kinetic model parameter determination in humans: the lumped constants and rate constants for [18F]fluorodeoxyglucose and [11C]deoxyglucose. Journal of Cerebral Blood Flow and Metabolism 1985;5:179–92.
[72] Tsui WH, Rusinek H, VanGelder P, Lebedev S. Analyzing multimodality tomographic images and associated regions of interest with MIDAS. SPIE Proceedings on Medical Imaging: Image Processing 4322 (in press).
[73] Freeborough PA, Fox NC, Kitney RI. Interactive algorithms for the segmentation and quantitation of 3D MRI brain scans. Computer Methods and Programs in Biomedicine 1997;53:15–25.
[74] Alpert NM, Bradshaw JF, Kennedy D, Correia JA. The principal axes transformation—a method for image registration. J Nucl Med 1990;31:1717–22.
[75] Rusinek H, Tsui WH, Levy AV, Noz ME, de Leon MJ. Principal axes and surface fitting methods for three-dimensional image registration. J Nucl Med 1993;34:2019–24.
[76] Convit A, de Leon MJ, Hoptman MJ, Tarshish C, De Santi S, Rusinek H. Age-related changes in brain. I. Magnetic resonance imaging measure of temporal lobe volumes in normal subjects. Psychiatric Quarterly 1995;66:343–55.
[77] Amaral DG, Insausti R. Hippocampal formation. In: Paxinos G, editor. The human nervous system. San Diego: Academic Press, Inc., 1990. pp. 711–55.
[78] Minoshima S, Frey KA, Foster NL, Kuhl DE. Preserved pontine glucose metabolism in Alzheimer's disease: a reference region for functional brain image (PET) analysis. Journal of Computer Assisted Tomography 1995;19:541–7.
[79] Ishii K, Yamji S, Mori E. Cerebellar metabolic reduction in Alzheimer's Disease and Data Normalization. J Nucl Med 1998;39:375–6.
[80] Ishii K, Sasaki M, Matsui M, Sakamoto S, Yamaji S, Hayashi N, Mori T, Kitagaki H, Hirano N, Mori E. A diagnostic method for suspected Alzheimer's disease using H_2 ^{15}O positron emission tomography perfusion Z score. Neuroradiology 2000;42:787–94.
[81] Vander Borght T, Minoshima S, Giordani B, Foster NL, Frey KA, Berent S, Albin RL, Koeppe RA, Kuhl DE. Cerebral metabolic differences in Parkinson's and Alzheimer's disease matched for dementia severity. J Nucl Med 1997;38:797–802.
[82] Albin RL, Minoshima S, DAmato CJ, Frey KA, Kuhl DE, Sima AAF. Fluoro-deoxyglucose positron emission tomography in diffuse lewy body disease. Neurol 1996;47:462–6.
[83] Videen TO, Perlmutter JS, Mintun MA, Raichle ME. Regional correction of positron emission tomography data for the effects of cerebral atrophy. Journal of Cerebral Blood Flow & Metabolism 1988;8:662–70.
[84] Meltzer CC, Leal JP, Mayberg HS, Wagner HN, Frost JJ. Correction of PET data for partial volume effects in human cerebral cortex by MR imaging. Journal of Computer Assisted Tomography 1990;14:561–70.
[85] Meltzer CC, Zubieta JK, Brandt J, Tune LE, Mayberg HS, Frost JJ. Regional hypometabolism in Alzheimer's disease as measured by positron emission tomography after correction for effects of partial volume averaging. Neurol 1996;47:454–61.
[86] Ibanez V, Pietrini P, Alexander GE, Furey ML, Teichberg D, Rajapakse JC, Rapoport SI, Schapiro M, Horwitz B. Regional gluose metabolic abnormalities are not the result of atrophy in Alzheimer's disease. Neurol 1999;50:1585–93.
[87] Saunders JK, Smith IC, MacTavish JC, Rydzy M, Peeling J, Sutherland E, Lesiuk H, Sutherland GR. Forebrain ischemia studied using magnetic resonance imaging and spectroscopy. NMR in Biomedicine 1989;2:312–6.
[88] Juottonen K, Laakso MP, Insausti R, Lehtovirta M, Pitkanen A, Partanen K, Soininen H. Volumes of the entorhinal and perirhinal cortices in Alzheimer's disease. Neurobiology of Aging 1998;19:15–22.
[89] Kennedy AM, Frackowiak RSJ, Newman SK, Bloomfield PM, Seaward J, Roques P, Lewington G, Cunningham VL, Rossor MN. Deficits in cerebral glucose metabolism demonstrated by positron emission tomography in individuals at risk of familial Alzheimer's disease. Neuroscience Letters 1995;186:17–20.
[90] Detoledo-Morrell L, Sullivan MP, Morrell F, Wilson RS, Bennett DA, Spencer S. Alzheimer's disease: in vivo detection of differential vulnerability of brain regions. Neurobiology of Aging 1997;18:463–8.
[91] Laakso MP, Lehtovirta M, Partanen K, Riekkinen PJ, Soininen H. Hippocampus in Alzheimer's disease: a 3-year follow-up MRI Study. Biological Psychiatry 2000;47:557–61.
[92] Hof PR, Bierer LM, Perl DP, Delacourte A, Buee L, Bouras C, Morrison JH. Evidence for early vulnerability of the medial and inferior aspects of the temporal lobe in an 82-year-old patient with preclinical signs of dementia: regional and laminar distribution of neurofibrillary tangles and senile plaques. Arch Neurol 1992;49:946–53.
[93] Giannakopoulos P, Hof PR, Michel JP, Guimon J, Bouras C. Cerebral cortex pathology in aging and Alzheimer's disease: a quantitative survey of large hospital-based geriatric and psychiatric cohorts. Brain Research Reviews 1997;25:217–45.
[94] Ikeda M, Tanabe H, Nakagawa Y, Kazui H, Oi H, Yamazaki H, Harada K, Nishimura T. MRI-based quantitative assessment of the hippocampal region in very mild to moderate Alzheimer's disease. Neuroradiology 1994;36:7–10.
[95] Mielke R, Kessler J, Szelies B, Herholz K, Wienhard K, Heiss WD. Normal and pathological aging—findings of positron-emission-tomography. J Neural Transm 1998;105:821–37.
[96] Ono M, Kublik S, Abernathey CD. Atlas of the cerebral sulci. New York: Thieme Medical Publishers, Inc., 1990.
[97] Terry RD, Peck A, De Teresa R, Schechter K, Horoupian DS. Some morphometric aspects of the brain in senile dementia of the Alzheimer type. Ann Neurol 1981;10:184–92.
[98] de la Monte SM. Quantitation of cerebral atrophy in preclinical and end-stage Alzheimer's disease. Ann Neurol 1989;25:450–9.
[99] Rusinek H, de Leon MJ, George AE, Stylopoulos LA, Chandra R, Smith G, Rand T, Mourino M, Kowalski H. Alzheimer disease: measuring loss of cerebral gray matter with MR imaging. Radiology 1991;178:109–14.